THE JOURNAL OF PHYSICAL CHEMISTRY B

Article

Cite This: J. Phys. Chem. B 2018, 122, 10582−10592

pubs.acs.org/JPCB

Ion−Molecule Complex Dissociation and Formation Dynamics in LiCl Aqueous Solutions from 2D IR Spectroscopy

Rongfeng Yuan, Chang Yan, and Michael Fayer*

Department of Chemistry, Stanford University, Stanford, California 94305, United States

Supporting Information

ABSTRACT: Ion−molecule complex dynamics as well as water dynamics in concentrated lithium chloride (LiCl) solutions are examined using ultrafast two-dimensional infrared (2D IR) spectroscopy with the CN stretching mode of methyl thiocyanate (MeSCN) as the vibrational probe. In pure water, MeSCN has a narrow symmetric absorption line shape. 2D IR spectral diffusion measurements of the CN stretch give the identical time dependence of water dynamics, as previously observed using the OD stretch of HOD in H_2O. In concentrated LiCl solutions, the IR absorption spectrum of MeSCN displays two distinct peaks, one corresponding to water H-bonded to the N lone pair of MeSCN (W) and the other corresponding to Li^+ associated with the N (L). These two species are in equilibrium, and switching of the CN bonding partner from Li^+ to H_2O and vice versa was observed and explicated with 2D IR chemical exchange spectroscopy. The MeSCN·Li^+ complex dissociation time constant, τ_{LW}, and the MeSCN·H_2O dissociation time constant, τ_{WL}, were determined. The observed τ_{LW} chemical exchange dissociation time constant changes from 60 to 40 ps as the LiCl concentration decreases from ∼10.7 to ∼7.7 M, mainly due to the increase of the water concentration as the LiCl concentration is reduced. The observed time constants are independent of the model for the chemical reaction. With the assumption of a simple chemical equation, MeSCN·Li^+ + H_2O ⇄ MeSCN·H_2O + Li^+, the equilibrium equation rate constants were obtained from the observed chemical exchange time constants. It was determined that the equilibrium rate constants barely change even though the viscosity changes by a factor of 2 and the ionic strength changes by a factor of 1.4. Extrapolation to dilute LiCl solution estimates the τ_{LW} to be ∼30 ps. The orientational relaxation (anisotropy decay) of both the W and L complexes was measured using polarization selective 2D IR experiments. The lithium-bonded species undergoes orientational relaxation ∼3 times slower than the water-bonded species in each LiCl solution studied. The difference demonstrates the distinct interactions with the medium experienced by the neutral and charged species in the concentrated salt solutions.

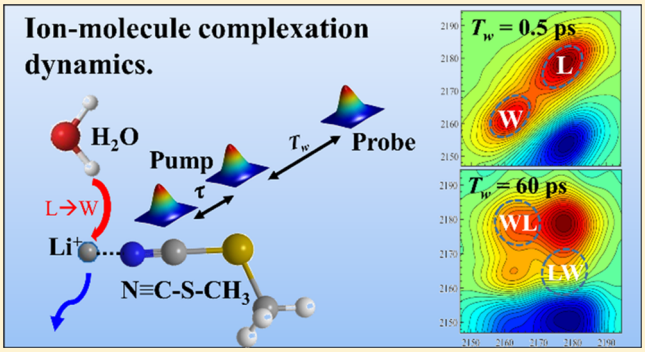

Downloaded via STANFORD UNIV on December 5, 2018 at 18:32:25 (UTC).
See https://pubs.acs.org/sharingguidelines for options on how to legitimately share published articles.

I. INTRODUCTION

Aqueous salt solutions occur widely in systems ranging from industrial processes to biological materials. Prominent examples include batteries and the salt balance in living organisms. The properties of aqueous electrolyte solutions involve the dynamics of water and the dynamics of ions. The dynamics are influenced by ion−ion interaction and ion−molecule interactions.[1] Water dynamics have been intensively examined by various techniques, including NMR,[2] neutron scattering,[3] Raman spectroscopy,[4] and ultrafast IR spectroscopies.[5−7] For ion dynamics, ultrafast IR spectroscopies have also been applied to examine various important problems in the field. For instance, ion pairs are common in electrolyte solutions, especially in concentrated salt solutions.[8−10] The pairing dynamics among lithium cations and thiocyanate anions in dimethylformamide solution were studied with two-dimensional infrared (2D IR) spectroscopy using thiocyanate anions as the IR probe.[11,12] Ion−molecule interactions are important in many processes[13−16] and have also been studied with ultrafast IR spectroscopy. MeSCN·Li^+ complexation in acetonitrile solution was studied using MeSCN as the IR probe.[17] HOD was used as the vibrational probe in aqueous solutions to examine hydrogen bond exchange times for water−anion complexes; the exchange time was found to be ∼10 ps.[18,19]

Polar organic molecules can dissolve in aqueous salt solutions. They can form H-bonds with water as well as associate with ions. Water-associated molecules and ion-associated molecules will be in equilibrium. A molecule will undergo chemical exchange, with a bound water molecule being replaced by an ion and vice versa. To the best of our knowledge, there is no information on the dynamics and concentration dependence of the chemical exchange. The dynamics of molecule−water/molecule−ion chemical exchange in concentrated salt solutions is becoming increasingly important due to such solutions' potential

Received: September 6, 2018
Revised: October 24, 2018
Published: October 26, 2018

ACS Publications © 2018 American Chemical Society

DOI: 10.1021/acs.jpcb.8b08743
J. Phys. Chem. B 2018, 122, 10582−10592

applications in battery development and energy-storage systems.[20,21]

Among numerous aqueous salt solutions, lithium chloride solutions have been extensively studied as a model system for water dynamics for decades due to their extraordinary solubility.[3,22−24] In dilute lithium chloride solutions, lithium cations are coordinated by ∼4 water molecules and chloride anions are solvated by ∼6 water molecules.[22] In concentrated solutions, however, water is so scarce that ion pairs of Li^+ and Cl^- are common, and water also forms bridges between Li^+ and Cl^-.[22,24] Molecular dynamics simulations have suggested that the hydrogen bond number decreases as much as ∼70%, although hydrogen bond lengths and strengths are similar to those found in pure water.[23]

In this paper, we examine ion−molecule complexation in LiCl solutions. The association of water and Li^+ with methyl thiocyanate (MeSCN) is investigated using the CN stretch of MeSCN as the vibrational probe. MeSCN is a small neutral molecule with a relatively strong CN stretch absorption band. Compared to the usual OD or OH stretch of HOD molecules used to study water dynamics,[25−27] the narrow bandwidth (full-width at half-maximum (FWHM) 10.5 cm^{-1}) and long vibrational lifetime (35 ps) are very useful in distinguishing different bonding environments and tracking relatively slow dynamics. First, it is shown that MeSCN is an excellent probe for water dynamics in pure water by using 2D IR to measure the CN stretch spectral diffusion. The results give the same spectral diffusion time constants as those found using the OD stretch of HOD in water.[26,27]

The linear Fourier transform infrared (FT-IR) absorption spectrum of the CN stretch of MeSCN in concentrated LiCl solutions displays two absorption bands, which are assigned to MeSCN·H_2O and MeSCN·Li^+ complexes. Chemical exchange between the two complexes was observed on the tens of picoseconds time scale by 2D IR spectroscopy through the growth of off-diagonal peaks in the time-dependent 2D spectra. The system was studied as a function of the LiCl concentration to determine the concentration-dependent dissociation rate of the MeSCN·Li^+ complex. It is shown that the dissociation rate can be extrapolated to the dilute limit. In addition, the orientational relaxation time of both MeSCN·H_2O and MeSCN·Li^+ were measured. The orientational relaxation time of the two complexes are very different, reflecting the distinct interactions experienced by the neutral and charged species.

II. EXPERIMENTAL METHOD

II.I. Sample Preparation. Lithium chloride (LiCl) (anhydrous, >99%) and methyl thiocyanate (>97%) (MeSCN) were purchased from Sigma-Aldrich and were used without further purification. LiCl solutions were prepared by mixing LiCl and H_2O based on mass to give the molar ratio between the Li^+ cation and water molecules values of 1:4, 1:5, and 1:6. MeSCN was added later to the desired concentration, 0.2 mol/L (M) in H_2O, and 0.10−0.15 M in LiCl solutions.

Densities were measured using a 5.00 mL pyknometer at the IR experimental temperature 24 °C. Kinematic viscosities of the solutions with MeSCN were measured using an Ubbelohde viscometer at 24 °C. Dynamic viscosities are obtained as the product of the density and the kinematic viscosity.

Infrared absorption spectra were measured using a Thermo Scientific Nicolet 6700 FT-IR spectrometer with 0.24 cm^{-1} resolution. Solutions with and without MeSCN were measured, and scaled subtraction of the two spectra yields the pure absorption line of the MeSCN in the solutions.

II.II. Two-Dimensional IR Vibrational Echo Spectroscopy. The following is a brief description of the 2D IR spectroscopy system used in this study. Details of the setup have been reported previously.[28] A mid-IR optical parametric amplifier pumped by a Ti:Sapphire regenerative amplifier produced ∼160 fs pulses with ∼30 μJ pulse energy centered at 2160−2170 cm^{-1} depending on the sample. The mid-IR pulse was then split into a strong pump pulse and a weak probe pulse. The pump pulse passes through an acousto-optic mid-IR Fourier-domain pulse shaper,[29,30] which forms it into two collinear pulses with a variable time delay between them of τ. After the pulse shaper, the energy in the two pump pulses is ∼12 μJ. The probe pulse crosses with the two pump pulses in the sample after a waiting time T_w, and the echo pulse is generated collinear with the probe pulse. The probe pulse, pulse 3 in the echo pulse sequence, induces the polarization that gives rise to the echo pulse and also serves as the local oscillator for heterodyne detection of the echo.

To understand how 2D IR works, first consider the vibrational absorption spectrum with a single peak. Intermolecular interactions between the molecules and the environment will in part determine the vibrational frequency of a mode that is used as a vibrational probe. Because different molecules have distinct environments, they will have different intermolecular interactions and thus vibrational frequencies. This range of vibrational frequencies is responsible for the inhomogeneous broadening of the vibrational absorption line. However, the structures of the environments of molecules in liquids and other media are constantly changing. This leads to time evolution of vibrational frequency, which is called spectral diffusion. Thus, measurement of spectral diffusion is a measurement of the time dependence of the structure of the system. This information cannot be obtained from linear absorption spectrum, but can be measured as spectral diffusion via 2D IR.

Qualitatively, 2D IR works as follows. There are four pulses in the pulse sequence, three input pulses that generate a nonlinear polarization that gives rise to the emission of a fourth pulse the vibrational echo. Basically, the first two pulses label and store the initial frequencies, which give to the horizontal axis of 2D spectrum, ω_τ. During the time between the second and third pulses, T_w, the structure evolves. The third pulse and echo read out the final frequencies, which is the vertical axis ω_m.

Spectral diffusion (vibrational frequency evolution) causes the gradual loss of correlation between the initial frequencies, ω_τ, and the final frequencies, ω_m. The 2D spectrum is elongated along the diagonal of the 2D spectrum, and it will become increasingly round as T_w is increased. The change in shape of the spectra with T_w is analyzed quantitatively with the center line slope (CLS) method, which gives the normalized frequency−frequency correlation function (FFCF) from the T_w dependence of the 2D spectral shape.[31,32] From the CLS decay curve and the linear absorption spectrum, the full FFCF is obtained. The FFCF, $C(t)$, is modeled as a multiexponential decay.

$$C(t) = \langle \delta\omega(t)\, \delta\omega(0) \rangle = \sum_i \Delta_i^2 \exp(-t/\tau_i) \quad (1)$$

Δ_i is the frequency fluctuation amplitude of each component and τ_i is its associated time constant. Therefore, determining the FFCF gives the time constants and amplitudes of the various dynamical processes occurring in the medium.[26,27,33] Further

DOI: 10.1021/acs.jpcb.8b08743
J. Phys. Chem. B 2018, 122, 10582−10592

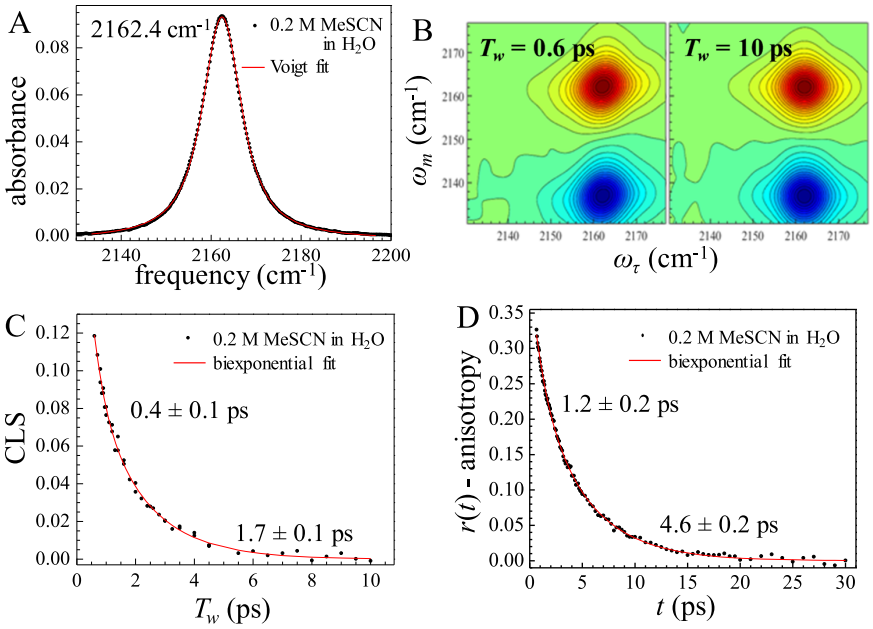

Figure 1. (A) Linear IR absorption spectrum of 0.2 M MeSCN in H_2O (black dots) and its Voigt fit (red line). Its Lorentzian FWHM is 9.2 cm^{-1}, whereas the Gaussian FWHM is 3.6 cm^{-1}. (B) Examples of 2D spectra of this system at two waiting times (T_w). (C) The CLS extracted from the 2D IR experiments (black dots) and its biexponential fit (red line). (D) The anisotropy (black dots) at the peak center extracted from PSPP experiments and its biexponential fit (red line).

details concerning the FFCF are given in the Supporting Information.

The main application of 2D IR spectroscopy in this paper is to observe chemical exchange,[34] i.e., the interconversion of the complexes MeSCN·H_2O and MeSCN·Li^+ one to the other. Chemical exchange spectroscopy (CES) has been applied to multiple studies, including the rate of isomerization around a carbon−carbon single bond,[35] the switching between well-defined protein structural substates,[36] and ion−water hydrogen bond switching.[18,19] The observation of chemical exchange requires two spectroscopic absorption lines originating from the same probe molecular vibration. Here, the two lines originate from two MeSCN complexes. In addition to spectral diffusion within each line, the vibrational mode makes large frequency jumps from one line to the other. The different FT-IR spectra of the two species produce two bands on the diagonal of the 2D IR spectrum. The beginning of the pulse sequence labels the complexes with their frequencies. When these complexes turn from one to the other, the CN stretch frequency changes, from the frequency of one complex to the other. The exchange produces off-diagonal peaks in the spectrum, which are read out by the echo. As time proceeds, the off-diagonal peaks grow in. Detailed analysis of the growth of the off-diagonal peaks, as presented below, gives the chemical exchange times.[37]

II.III. Polarization Selective Pump Probe (PSPP). The PSPP experiments were performed using the same ultrafast IR setup. PSPP tracks the decay of the probe transmission with polarizations parallel and perpendicular to the pump pulse polarization. The parallel and perpendicular components of the probe signal, $S_{\parallel}(t)$ and $S_{\perp}(t)$, can be expressed in terms of population relaxation, $P(t)$, and the second Legendre polynomial orientational correlation function, $C_2(t)$.[38,39]

$$S_{\parallel}(t) = P(t)[1 + 0.8C_2(t)] \tag{2}$$

$$S_{\perp}(t) = P(t)[1 - 0.4C_2(t)] \tag{3}$$

In terms of these, the population relaxation and reorientational relaxation are

$$P(t) = S_{\parallel}(t) + 2S_{\perp}(t) \tag{4}$$

$$r(t) = \frac{S_{\parallel}(t) - S_{\perp}(t)}{S_{\parallel}(t) + 2S_{\perp}(t)} \tag{5}$$

$r(t)$ is the anisotropy with $r(t) = 0.4C_2(t)$.

In the PSPP experiments, the input polarization of the probe was horizontal. A half wave plate and a polarizer set the polarization of pump to 45° relative to horizontal. Following the sample, the probe pulse was resolved either parallel or perpendicular to the polarization of the pump using a polarizer in a computer-controlled rotation mount. Care was taken to make sure that the probe spectra in the parallel and perpendicular polarizations were identical in amplitude in the absence of the pump pulse.

III. EXPERIMENTAL RESULTS

III.I. Linear and 2D IR Spectroscopies of MeSCN in Pure Water. Although MeSCN is a neutral organic molecule, it dissolves in water reasonably well. The ability to form hydrogen bonds between the nitrogen lone pair and water helps the solvation. This bonding opens the window for detecting water dynamics through CN stretch, as is the case for selenocyanate anions.[40,41] In pure water, MeSCN has a narrow symmetric band centered at 2162.4 cm^{-1} with full-width at half-maximum (FWHM) of 10.5 cm^{-1}. Figure 1A shows that a Voigt line shape fits the absorption spectrum well. 2D IR experiments were conducted on 0.2 M MeSCN in water; two examples of 2D spectra are shown in Figure 1B. The red bands (positive going) arise from the ground state to first excited vibrational state (0 to 1) transition. The blue bands arise from the 1 to 2 transition. They are shifted to lower frequency along the ω_m axis by the vibrational anharmonicity. Small heating signals from water and

DOI: 10.1021/acs.jpcb.8b08743
J. Phys. Chem. B 2018, 122, 10582−10592

the probe were subtracted before CLS analysis (see Supporting Information for details).

Figure 1C shows the experimental CLS data (points) obtained from analyzing many 2D spectra like those shown in Figure 1B. The data are fit very well with a biexponential function. Because of the long CN vibrational lifetime, it was possible to take data over the full time span of the dynamics. The biexponential fit gives the time constants 0.4 ± 0.1 and 1.7 ± 0.1 ps. These values are identical to the results obtained using the OD stretch of HOD as the vibrational probe in H_2O.[5,26,27,33] Therefore, the CN stretch of MeSCN is a very useful probe of water dynamics. The consensus is that the fast process corresponds to the local hydrogen bond fluctuations, mainly length fluctuations, whereas the slower process describes the global hydrogen bond network randomization.[27]

PSPP experiments were also performed on the sample, and the vibrational lifetime was determined to be 35 ps. This is in contrast to the OD stretch, which has a lifetime of 1.7 ps.[5,26,27,33] The long lifetime of the CN stretch is essential to the experiments discussed below. Orientational relaxation of MeSCN in pure water was obtained using eq 5. The anisotropy decay (points) is shown in Figure 1D. The anisotropy was fit with a biexponential decay (solid curve) with 1.2 and 4.6 ps as time constants. The 1.2 ps process is associated with a "wobbling-in-a-cone" motion. The probe molecule can undergo angular fluctuations within a restricted cone of angles on a short time scale[41−43] before the orientation fully randomizes.[41] The 4.6 ps decay component corresponds to the complete orientational randomization of the MeSCN. In summary, we have shown that MeSCN is a faithful probe of water dynamics with a long vibrational lifetime. We also characterized its reorientational dynamics in pure water, which will be compared with the values in LiCl solutions.

III.II. Linear IR Spectra of MeSCN in LiCl Solution. When MeSCN is dissolved in concentrated LiCl solutions, the linear IR absorption spectra have an additional blue-shifted peak at ~2179 cm^{-1}. As LiCl concentration increases, the blue-shifted peak increases in amplitude, as shown in Figure 2, where the four spectra are normalized at 2162 cm^{-1} peak center. This trend enables us to assign the new peak to be the Li^+-associated component, whereas the 2162 cm^{-1} peak corresponds to MeSCN still associated with water. As shown in Table 1, the FWHMs of the two peaks are larger than that in pure water, indicating more heterogeneous environments for the probe. As

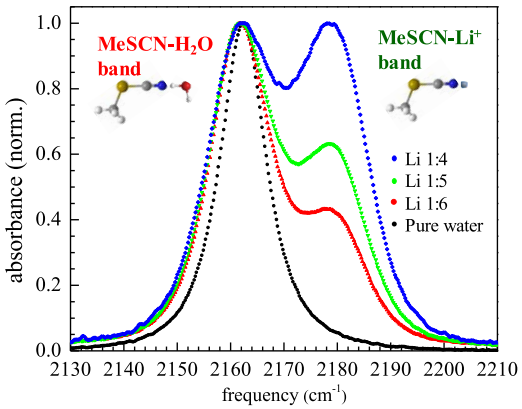

Figure 2. Background-subtracted linear IR absorption spectra of the CN stretch of MeSCN in water and LiCl solutions whose concentration is labeled as the molar ratio between the Li^+ cation and water.

in pure water, the water-associated peak is a result of hydrogen bond formation between the nitrogen lone pair (H-bond acceptor) and the H of a water molecule (H-bond donor). The nitrogen will interact strongly with a lithium cation with its very high positive charge density. This strong interaction is sometimes called a "lithium bond", and lithium cation's high charge density plays a significant role.[44]

III.III. Two-Dimensional IR Chemical Exchange Spectroscopy. As the LiCl concentration increases, ions are closer together. Smith et al. found that beyond the dilute (Debye−Hückel) regime, the screening length becomes longer as concentration increases.[45] The longer screening length indicates long-range interactions and likely slower dynamics due to more restrictive forces. This is partly evidenced by the significant increase of viscosity of concentrated LiCl solutions compared to pure water, which is shown in Table 1.

We conducted ultrafast IR experiments on MeSCN in LiCl solutions and observed that the two populations reflected in the linear IR absorption spectra (Figure 2) underwent chemical exchange, as shown in Figure 3. Figure 3 displays data for three concentrations at three times. The data for each concentration are a row in the figure. On the basis of simple inspection of the growth of the cross peaks in the 2D spectra, chemical exchange happens on the order of tens of picoseconds.

To quantify the dynamics, we need a kinetic model to analyze the data. Take the results from LiCl 1:4 H_2O solution as an example. Shown in Figure 4C left, at the early $T_w = 0.6$ ps, when basically no chemical exchange has occurred, the spectrum has two diagonal peaks, labeled W_{01} (water-bound population) and L_{01} (lithium-bound population), corresponding to the vibrational echo emission at the 0−1 transitions, and two negative-going peaks corresponding to the 1−2 transitions, labeled W_{12} (not shown) and L_{12}. The latter two peaks are shifted to lower frequencies along the echo emission (vertical) axis ω_m by their anharmonicity (~25 cm^{-1}). As T_w increases, exchange peaks, WL_{01} (initial state is W and final state is L) and LW_{01}, start to grow and become of almost equal amplitude to the diagonal peaks at $T_w = 60$ ps (Figure 4C right). Exchange peaks in the 1−2 region, for example WL_{12}, also grow at the same rate.[34]

To connect the observed chemical exchange data to chemical reactions, we assume the chemical equilibrium equation

$$\mathrm{MeSCN{\cdot}Li^+ + H_2O \underset{k_b}{\overset{k_f}{\rightleftarrows}} MeSCN{\cdot}H_2O + Li^+} \quad (6)$$

to model the process. The equation shows the switching of the bonding partner for MeSCN from water to Li^+ and vice versa, with two rate constants k_f and k_b (below, eq 6 will be shown to be a valid description of the system). The MeSCN concentration is 0.10−0.15 mol/L, whereas the concentrations of Li^+ and H_2O are at least 7.6 and 42 mol/L, respectively. Therefore, $[Li^+]$ and $[H_2O]$ are essentially constant in the samples, and the eq 6 can be simplified to eq 7, which is convenient for kinetic model analysis of the chemical exchange data.

$$\mathrm{MeSCN{\cdot}Li^+} \underset{k_{WL}}{\overset{k_{LW}}{\rightleftarrows}} \mathrm{MeSCN{\cdot}H_2O}$$

$$k_{LW} = k_f[H_2O], \quad k_{WL} = k_b[Li^+] \quad (7)$$

$MeSCN{\cdot}Li^+$ is called L (lithium associated) and $MeSCN{\cdot}H_2O$ is called W (water associated). In the context of the 2D chemical exchange spectra, all molecules in the W diagonal peak at $T_w = 0$ can be in either W or the WL off-diagonal peak at later T_w no matter how many exchange events occur. The WL off-diagonal

DOI: 10.1021/acs.jpcb.8b08743
J. Phys. Chem. B 2018, 122, 10582−10592

Table 1. Experimental Parameters

	1:4[a]	1:5[a]	1:6[a]	H_2O[b]
FWHM-W (cm^{-1})	15.1 ± 0.3	14.1 ± 0.3	13.5 ± 0.3	
FWHM-H_2O				10.5 ± 0.2
FWHM-L (cm^{-1})	15.8 ± 0.3	15.2 ± 0.3	14.8 ± 0.3	
τ_w (ps)[c]	25.6 ± 0.8	30.5 ± 0.8	31.9 ± 0.7	
τ_{H_2O} (ps)[c]				35.0 ± 0.2
τ_L (ps)[c]	49 ± 4	47 ± 4	51 ± 6	
τ_{WL} (ps)[d]	92 ± 9	126 ± 10	154 ± 15	
τ_{LW} (ps)[d]	59 ± 5	50 ± 5	41 ± 4	
τ_{ex} (ps)[e]	35 ± 2	35 ± 2	32 ± 2	
k_b (ns^{-1})	1 ± 0.1	0.9 ± 0.07	0.86 ± 0.06	
k_f (ns^{-1})	0.40 ± 0.04	0.45 ± 0.05	0.53 ± 0.06	
dyn. viscosity (cP)	6.29 ± 0.06	4.09 ± 0.06	3.11 ± 0.05	0.94 ± 0.03
eq. conc. ratio (W/L)[f]	1.6 ± 0.3	2.5 ± 0.4	3.8 ± 0.7	
$[Li^+]$ (mol/L)	10.7	8.98	7.72	
$[H_2O]$ (mol/L)	42.6	45.0	46.3	55.4
$\tau_{OR\text{-}W}$ (ps)[g]	14.9 ± 0.9	10.2 ± 0.6	8.4 ± 0.5	
$\tau_{OR\text{-}H_2O}$ (ps)[g]				4.6 ± 0.2
$\tau_{OR\text{-}L}$ (ps)[g]	54 ± 2	41 ± 2	36 ± 2	

[a]LiCl/H_2O ratio. [b]Pure H_2O. [c]CN stretch vibrational lifetime; $\tau_i = 1/k_i$. [d]Exchange times; $\tau_{ij} = 1/k_{ij}$. [e]$\tau_{ex} = 1/(k_{WL} + k_{LW})$. [f]Eq. conc. ratio (W/L): the equilibrium ratio of the W and L components concentrations. [g]$\tau_{OR\text{-}i}$: the orientational relaxation time constant of the ith component.

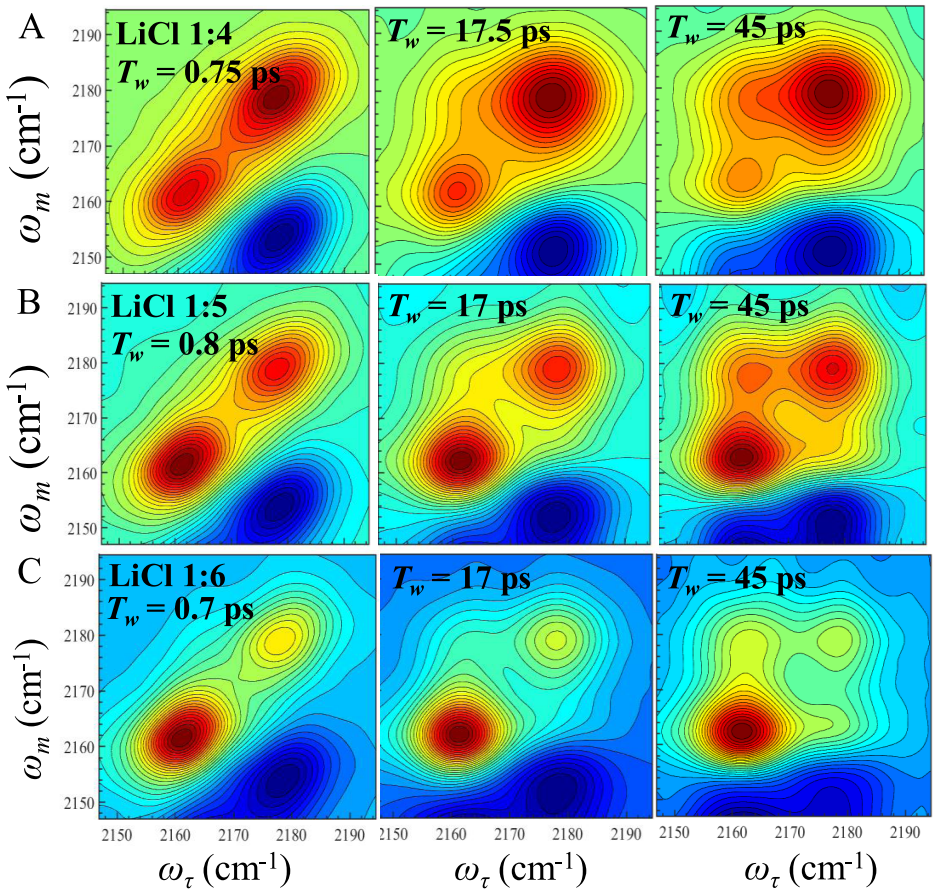

Figure 3. 2D spectra (isotropic) examples of LiCl solution at three concentrations. Rows (A), (B), and (C) correspond to molar ratio between Li^+ and H_2O being 1:4, 1:5, and 1:6, respectively.

peak arises from MeSCN molecules that started as W and became L. When they become L, the amplitude is increased in the WL off-diagonal peak not the L diagonal peak. Therefore, 2D IR spectroscopy is watching the progression from all of the molecules in W peak ($T_w = 0$) to eventual equilibrium between W and WL. The process of reaching equilibrium between L and LW is observed in the same way by growth of the off-diagonal LW peak.

A quantitative model was developed to account for the source and drain for the corresponding populations in the 2D spectra. A

DOI: 10.1021/acs.jpcb.8b08743
J. Phys. Chem. B 2018, 122, 10582−10592

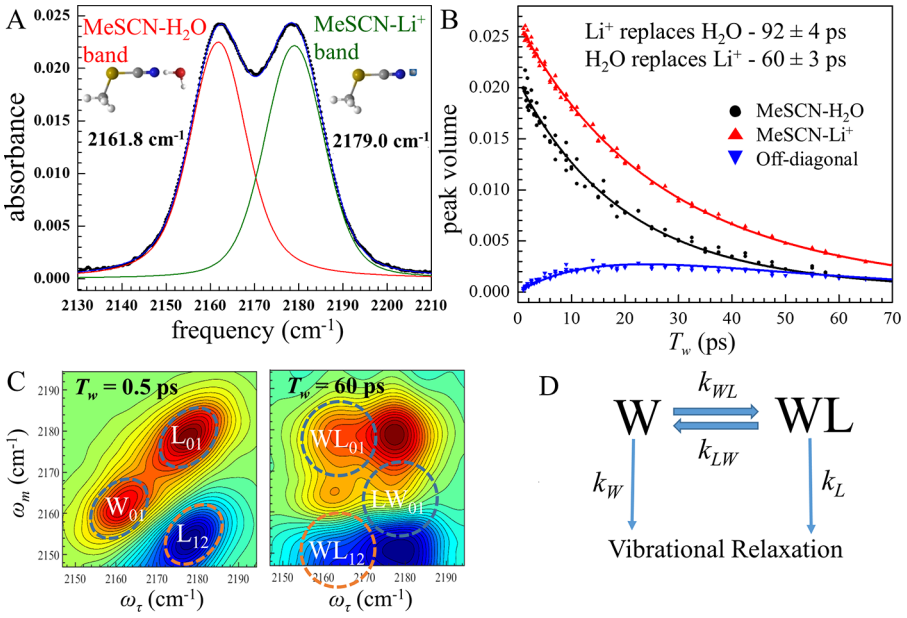

Figure 4. MeSCN in LiCl 1:4 H_2O solution. (A) The linear IR absorption spectrum of MeSCN in LiCl 1:4 H_2O solution (black dots) and the red curves are the fits using two Voigt functions. (B) The peak volumes extracted from the 2D spectra (dots) and the fits (solid curves) using the kinetic model. (C) Two examples of 2D spectra of LiCl 1:4 H_2O illustrating the effect of chemical exchange. (D) A schematic representation of the kinetic model.

schematic for equilibration between W and WL is shown in Figure 4D. The time-dependent population of W diagonal peak $N_W(t)$ will decrease because of the vibrational relaxation and conversion from W to WL. At the same time, back conversion from WL to W will repopulate W with some of the lost population. Vibrational relaxation to the ground state is reducing the population of all peaks. The off-diagonal peak WL time-dependent population, $N_{WL}(t)$, is described similarly, the only notable difference is that the vibrational relaxation rate is k_L, rather than k_W. The relations described above can be written as

$$\begin{pmatrix} \dot{N}_W \\ \dot{N}_{WL} \end{pmatrix} = \begin{pmatrix} -(k_W + k_{WL}) & k_{LW} \\ k_{WL} & -(k_L + k_{LW}) \end{pmatrix} \begin{pmatrix} N_W \\ N_{WL} \end{pmatrix} \tag{8}$$

where a dot indicates time derivative. Here, k_W and k_L are vibrational relaxation time constants for W and L species. k_{WL} and k_{LW} are exchange rates from W to L and L to W, which are connected by chemical equilibrium.

With the initial condition being $N_{WL}(t = 0) = 0$, the solutions of eq 8 are

$$N_W = \frac{N_W(t=0)}{2\Delta}\left[(\Delta + m)\exp\left(-\frac{1}{2}(s+\Delta)t\right) + (\Delta - m)\exp\left(-\frac{1}{2}(s-\Delta)t\right)\right]$$

$$N_{WL} = \frac{N_W(t=0)}{\Delta}k_{WL}\left[-\exp\left(-\frac{1}{2}(s+\Delta)t\right) + \exp\left(-\frac{1}{2}(s-\Delta)t\right)\right] \tag{9}$$

with

$$s = k_W + k_{WL} + k_{LW} + k_L$$

$$\Delta = \sqrt{s^2 - 4(k_W k_L + k_W k_{LW} + k_L k_{WL})}$$

$$m = k_W + k_{WL} - k_{LW} - k_L$$

$N_W(t = 0)$ is the initial value of the diagonal population and is just a scaling factor in the analysis. N_L and N_{LW} are calculated in the same way. Note that due to the nature of chemical equilibrium, $N_W(t = 0)k_{WL} = N_L(t = 0)k_{LW}$ is valid because $N_W(t = 0)$ and $N_L(t = 0)$ are equilibrium concentrations with equal pumping of the two absorption bands. The relation between them connects the two equilibria between a diagonal peak and the corresponding off-diagonal peak in the 2D spectra, which results in only one scaling factor. Additionally, $N_{WL} = N_{LW}$ is valid at all T_w because of the relation. That is the two off-diagonal peaks' populations are the same at all time. Therefore, there are three independent population evolutions with time, two diagonal peaks and one off-diagonal peak.

The population is directly proportional to the peak volumes in the 2D spectra. We use 2D Gaussian functions to model a single peak and use multiple 2D Gaussians to fit the entire 2D spectra to extract the peak volumes. However, there are a number of other necessary considerations to relate the peak volumes to the populations of different species. First, the polarizations of the IR pulses will affect the signal levels because of orientational relaxation, which in turn affect the peak volumes,[37] as in a PSPP experiment. To avoid the complication of including the time dependence of orientational relaxation of the species, we conducted vibrational echo experiments in both the parallel and perpendicular polarization configurations. Here, parallel and perpendicular have the same meaning as in PSPP, i.e., the pump pulses' polarization is either parallel or perpendicular to the probe and echo pulses' polarization. The isotropic signal can be obtained with the weighted average of the parallel and perpendicular signals with weighting ratio 1:2. In this way, orientational relaxation will not be involved in the fitting routine,

DOI: 10.1021/acs.jpcb.8b08743
J. Phys. Chem. B 2018, 122, 10582−10592

thus increasing the robustness of the procedure.[19,37] The polarization consideration will be clear from the material in Section III.IV where the mathematical expressions for the peak volumes with parallel and perpendicular polarizations are presented. Furthermore, transition dipole moments μ_W and μ_L could be different, and they will affect the relation between peak volumes and populations. μ_W^2/μ_L^2 was determined to be 0.70 ± 0.07 (details of the determination process are given in the Supporting Information).

Using the kinetic model with the considerations discussed above, the three populations' evolution data as a function of T_w were fit. Note that there are only four fitting parameters: $N_W(t = 0)$, which is just a scaling factor, k_W, k_L, and k_{WL} (or k_{LW}). As shown in Figure 4B, the model fit (solid curves) the three sets of data (points) for the LiCl 1:4 H_2O solution exceedingly well. One set of parameters put the solid curves through all three sets of data. This procedure was applied to two other LiCl concentration samples, and the peak volume fitting results are presented in Figure 5. Again, the fits are excellent. The extracted time constants are summarized in Table 1. The rate constants k_b and k_f were also calculated using eq 7 and are given in Table 1.

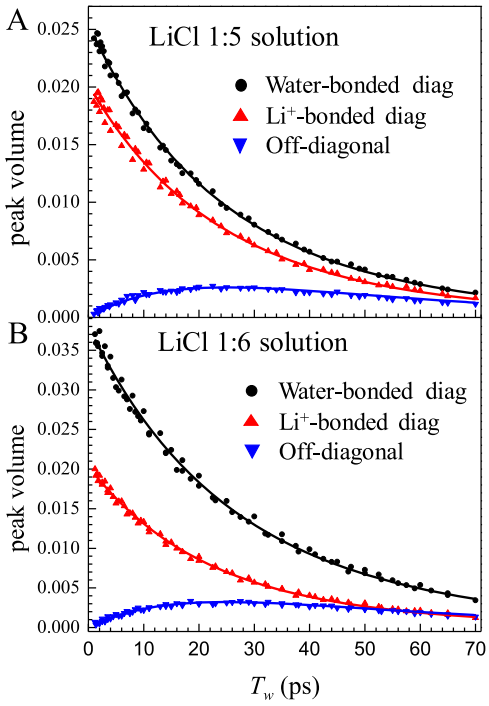

Figure 5. (A) and (B) are the peak volume evolutions of the 2D spectra collected in LiCl 1:5 and 1:6 H_2O solutions, respectively.

With the knowledge of the kinetic parameters, the chemical equilibrium independent of the spectroscopic observables is considered. Equation 8 can be modified into eq 10 for infinite vibrational lifetime. Here, N_W and N_L are the population of W and L species that are in chemical equilibrium.

$$\begin{pmatrix} \dot{N}_W \\ \dot{N}_L \end{pmatrix} = \begin{pmatrix} -k_{WL} & k_{LW} \\ k_{WL} & -k_{LW} \end{pmatrix} \begin{pmatrix} N_W \\ N_L \end{pmatrix} \tag{10}$$

with the initial condition $N_L(t = 0) = 0$, the solutions are

$$N_W = \frac{N_W(0)}{s}(k_{LW} + k_{WL}\exp(-st))$$

$$N_L = \frac{N_W(0)}{s}(k_{WL} - k_{WL}\exp(-st))$$

$$N_W + N_L = N_W(0),\ s = k_{LW} + k_{WL} \tag{11}$$

These equations describe the relaxation to the chemical equilibrium state if all of the molecules were W initially or if a sudden perturbation moved the concentration away from the equilibrium concentrations. For any initial condition, the relaxation time constant is $\tau_{ex} = 1/(k_{WL}+k_{LW})$. These values for the three concentrations are given in Table 1.

III.IV. Polarization Selective 2D IR Experiment. In a system involving chemical exchange, simply doing polarization selective pump probe (PSPP) is not enough to extract the orientational dynamics of the two species because chemical exchange mixes the two lifetimes and orientational relaxation times.[19,37] To disentangle the orientational dynamics from the chemical exchange, polarization selective 2D IR was used. As was mentioned in Section III.III, the 2D IR signals in the parallel and perpendicular configurations were measured at the same time in the same setup as used for the PSPP experiments. An example of 2D spectra of LiCl 1:4 H_2O solution at T_w = 45 ps is presented in Figure 6A. The most obvious difference is the different intensity of W diagonal peak between parallel and perpendicular spectra, which demonstrates unequal orientational relaxation for the W and L species. The effect of

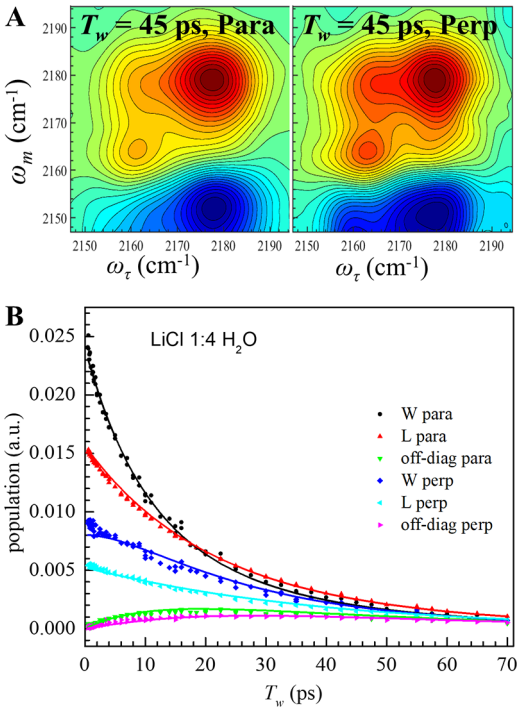

Figure 6. (A) Examples of polarization selective 2D spectra of LiCl 1:4 H_2O solution at waiting time 45 ps. (B) The population evolution of 2D spectra in the polarization selective 2D IR measurement done in LiCl 1:4 H_2O solution. W and L: water and lithium-bonded components, respectively. Off-diag means off-diagonal or cross peak in the 2D spectra. The suffix para and perp indicate measurement done in parallel and perpendicular configurations, respectively. Note that the population here is obtained by factoring out the transition dipole moment ratio from the peak volumes.

DOI: 10.1021/acs.jpcb.8b08743
J. Phys. Chem. B 2018, 122, 10582−10592

polarization control in 2D IR CES experiments has been described previously,[19,37] and we presented the final results (eq 12) that describe the population evolutions of diagonal and off-diagonal peaks under parallel and perpendicular configurations. Here, k_W, k_L, k_{WL}, and k_{LW} have the same meaning as in eqs 7 and 8. D_W and D_L are the orientational diffusion constants for species W and L, respectively. Note that eq 12 assumes that the reorientational relaxation of both species is single exponential without wobbling-in-a-cone behavior. For the systems discussed here, this assumption works well as will be shown below.

$$\begin{pmatrix} N_W(T_w) \\ N_{WL}(T_w) \end{pmatrix}_{para} = \left(e^{A\cdot T_w} + \frac{4}{5}e^{B\cdot T_w}\right) \times \frac{1}{3}\begin{pmatrix} N_W(0) \\ N_{WL}(0) \end{pmatrix}_{para}$$

$$\begin{pmatrix} N_W(T_w) \\ N_{WL}(T_w) \end{pmatrix}_{perp} = \left(e^{A\cdot T_w} - \frac{2}{5}e^{B\cdot T_w}\right) \times \frac{1}{3}\begin{pmatrix} N_W(0) \\ N_{WL}(0) \end{pmatrix}_{perp}$$

$$A = \begin{pmatrix} -(k_W + k_{WL}) & k_{LW} \\ k_{WL} & -(k_L + k_{LW}) \end{pmatrix}$$

$$B = \begin{pmatrix} -(k_W + k_{WL} + 6D_W) & k_{LW} \\ k_{WL} & -(k_L + k_{LW} + 6D_L) \end{pmatrix} \quad (12)$$

Both the parallel and perpendicular 2D IR spectra time dependence can be characterized in terms of two diagonal peaks and one off-diagonal peak, and overall there are six independent peak volume evolution curves. k_W, k_L, k_{WL}, and k_{LW} have already been obtained by the procedure described in Section III.III and are fixed here. D_W, D_L and an overall scaling factor are the only variables to fit the six curves simultaneously. The peak volume data (points) and the fitted curves (solid curves) are shown Figure 6B for the for the LiCl/H_2O ratio of 1:4. The data and fits for the other concentrations are similar. The model reproduces the polarization selective data exceptionally well. The fitting results are presented in Table 1 as $\tau_{OR\text{-}W}$ and $\tau_{OR\text{-}L}$. The orientational relaxation time, $\tau_{OR\text{-}H_2O}$, measured for MeSCN with standard PSPP experiments is also given. The orientational relaxation time is related to the orientational diffusion constant by $\tau_i = 1/6D_i$. As the LiCl concentration increases, the viscosity of the solution increases substantially (see Table 1). Both $\tau_{OR\text{-}W}$ and $\tau_{OR\text{-}L}$ increase as well, and they roughly follow the Stokes−Einstein−Debye relation. However, at all concentrations, the orientational relaxation time of the Li^+-associated MeSCN is much longer than the H_2O-associated species. The difference shows that the neutral and charged complexes experience distinct friction for rotation in the solutions, as is discussed further in the next section.

IV. DISCUSSION

The MeSCN and Li^+ complex exchange is important as the exchange provides an example of ion−molecule interaction dynamics in aqueous solution. As would be expected, as the LiCl concentration decreases from 1:4 to 1:6, τ_{WL} increases and τ_{LW} decreases (see Table 1). But this trend mainly originates from the change of [Li^+] and [H_2O] as k_b remains the same within experimental error, whereas k_f has only a slight increase with decreasing concentration, just outside of error. In addition, τ_{ex} remains the same for the three concentrations, although the solution viscosities decrease from 6.3 to 3.1 cP as the LiCl concentration decreases. The ionic strength also changes by a factor of ∼1.4. However, the consistencies of k_b and k_f with concentration demonstrate that ionic strength and viscosity have little or no impact on the rate of chemical exchange in the concentration range studied. The complexation dynamics can be extrapolated to dilute concentrations. Considering the experimental error bar, it is reasonable to treat k_f and k_b as constants and use them for dilute conditions where the water concentration is 55.4 mol/L. Then, $\tau_{LW} = 1/k_{LW} = 1/(k_f[H_2O]) = 39$ ps, which should be an upper limit. The other limit is to linearly extrapolate of k_f against water concentration regardless of the error bar. The extrapolation gives $\tau_{LW} = 22$ ps. It is plausible that the change of k_f will become slower as water concentration approaches 55.4 mol/L. Therefore, 22 ps is likely a lower limit for the dissociation time constant. Therefore, we estimated τ_{LW} to be ∼30 ps in dilute conditions.

The vibrational probe is the CN stretch of the MeSCN. The dominant interaction is between the nitrogen lone pair and a water molecule or a lithium cation. As can be seen in Figure 2, there is at most a very small shift in the MeSCN·H_2O spectrum in going from pure water to the high concentration LiCl solutions. The shift is 0.6 cm^{-1}, which is almost within the error bars of the measurement of the peak position. The concentrated solution does broaden the band, but only by ∼20% at the highest concentration and the broadening decreases as the concentration is lowered. 2D IR spectral diffusion measurements show that this broadening is caused by an increase in the inhomogeneous linewidth. In contrast, MeSCN in the non-hydrogen bonding solvent methylimidazole shifts the spectrum to lower frequency by 8 cm^{-1}. This shift is consistent with the model that has been put forward for the ion $SeCN^-$ that shows why a water hydrogen bonded to the N lone pair blue shifts the CN stretch frequency.[40] The model states that the blue shift is caused by an increase in the electron density in CN nominal triple bond. The nonaxial interactions, including those with Li^+, Cl^-, and water molecules, contribute to more diverse set of solvent configurations in salt solution and thus increase the inhomogeneous linewidth of W component. A similar argument applies to L complexes, where Li^+ forms an axial interaction with the nitrogen lone pair. Li^+ is very small with a high positive charge density. This interaction will further increase the electron density in the CN bond by moving electron density from the S−C bond, giving rise to the observed blue shift relative to the W complex.

As discussed above, τ_{LW} is the MeSCN·Li^+ complex lifetime, i.e., the time for a MeSCN initially bound to a Li^+ to become bound to a water. τ_{WL} is the time for an MeSCN initially bound to a water to become bound to a Li^+. It is important to note that a MeSCN initially bound to a water might switch water partners to another water one or more times before it becomes bound to a Li^+. The exchange experiment is insensitive to water to water switches. Such water to water switches can occur particularly as the Li^+ concentration is reduced. The same could occur with Li^+ to Li^+ switches, although this is less likely as the Li^+ concentration is lower than the water concentration.

There is a substantial difference in the orientational relaxation times of the MeSCN·Li^+ and MeSCN·H_2O complexes. $\tau_{OR\text{-}L}$ is ∼4 times slower than $\tau_{OR\text{-}W}$ at all concentrations studied. The rotational relaxation generally depends on the size of the molecule as in Stokes−Einstein−Debye relation, which has the orientational relaxation time proportional to the volume of the rotating species. Using Gaussian16A03,[46] we calculated the van der Waals volumes of the MeSCN·Li^+ and MeSCN·H_2O

DOI: 10.1021/acs.jpcb.8b08743
J. Phys. Chem. B 2018, 122, 10582−10592

complexes following the method published previously,[47] except that the complex geometry is optimized and volume is determined at the M062X/6-311+G(d,p) level. A solvent model for water is used in all calculations. The volume of a complex is defined where the electron density is greater than 0.001 e/a^3 where a is the Bohr radius. The calculation showed that the volumes of W and L complexes are 1.34 and 1.10 nm^3, respectively. Given this volume difference, the SEC equation would indicate that the L complex should rotate ∼20% faster than the W component. However, orientational relaxation also depends on the type of interaction between the rotating species and the surrounding liquid.[48] In strong electric fields, charged and neutral species with a permanent dipole will experience different resistances to rotation. The MeSCN is either a neutral or charged complex depending on its bonding partner. Their different orientational dynamics demonstrates distinct interactions with the surrounding salt solution. Ion pairs formed between Li^+ and Cl^- are common at the high concentrations used in the experiments.[22] The slow orientational relaxation of the Li^+ complex compared to the water complex is likely due to the stronger electrostatic interaction between Li^+ and the surrounding ions.

V. CONCLUDING REMARKS

In this study, we have shown that methyl thiocyanate (MeSCN) is an accurate probe for reporting water dynamics in aqueous environment. It has a narrow symmetric absorption line shape and has a long vibrational lifetime, 35 ps in pure water. CLS analysis applied to the 2D spectra taken in pure water to obtain the frequency−frequency correlation function yields a biexponential decay with 0.4 and 1.7 ps time constants, which are the same as those found using the OD stretch of HOD in water to measure the spectral diffusion dynamics.[5,26,27,33] For the probe HOD, the OD is H-bonded to a lone pair of an oxygen atom of a water molecule. The spectral diffusion dynamics reflect fluctuations of the H-bond. With the CN of MeSCN as the vibrational probe, a water molecule is H-bonded to the lone pair of the nitrogen atom. In either case, the spectral diffusion is associated with the collective dynamics of the water. The results indicate that the presence of the MeSCN does not substantially perturb the surrounding water dynamics, and having water H-bonded to a N lone pair rather than an O lone pair does not influence the observe spectral diffusion within experimental error.

In concentrated LiCl solution, the linear IR absorption of the CN stretch of MeSCN is split into two peaks: the lower frequency peak corresponds to water-bonded complex, whereas the higher frequency peak corresponds to lithium-bonded complex (see Figures 2 and 4A). Chemical exchange dynamics and orientational relaxation were measured for the two species in solutions with three LiCl concentrations (molar ratios of Li^+ to H_2O of 1:4, 1:5, and 1:6).

MeSCN·Li^+ and MeSCN·H_2O complex dynamics were obtained with 2D IR chemical exchange spectroscopy through detailed analysis of the growth of off-diagonal peaks in the 2D IR spectra (see Figures 3 and 4C). The rates were determined by a kinetic model. τ_{LW} (Li^+ to water complex) decreased from ∼60 to ∼40 ps when the LiCl concentration was decreased from 1:4 to 1:6. The change mainly originates from the increase in water concentration. τ_{LW} is the lifetime of the MeSCN−Li^+ complex.

The analysis also gives the rate constants k_f and k_b. Both k_f and k_b are almost constant with concentration, even though viscosity of solution changes by a factor of 2 and ionic strength varies by a factor of 1.4. This demonstrates that chemical exchange is at most weakly dependent on these two factors. Thus, we can extrapolate this result to dilute salt solution and estimate τ_{LW} to be ∼30 ps.

Finally, orientational relaxation dynamics of both the water-bonded and lithium-bonded complexes were measured. The Li^+ complex undergoes orientational relaxation ∼4 times slower than the water complex in each LiCl solution examined, although the Li^+ complex is ∼20% smaller in volume than the water complex. The slower reorientation of the Li^+ complex is likely due to strong electrostatic interactions with the surrounding salt solution. It is interesting to note that the water complex orientational relaxation time is much faster than τ_{WL}, whereas the Li^+ orientational relaxation time is approximately the same as τ_{LW}. Thus, the water complex randomizes its orientation much faster than exchanging water for Li^+, whereas the Li^+ complex exchanges Li^+ for water without necessarily having randomized its orientation.

■ ASSOCIATED CONTENT

Supporting Information

The Supporting Information is available free of charge on the ACS Publications website at DOI: 10.1021/acs.jpcb.8b08743.

Frequency−frequency correlation function (FFCF); determination of transition dipole ratio; heating background subtraction method (PDF)

■ AUTHOR INFORMATION

Corresponding Author

*E-mail: fayer@stanford.edu. Phone: 650 723-4446.

ORCID

Rongfeng Yuan: 0000-0002-6572-2472
Chang Yan: 0000-0001-9735-3002
Michael Fayer: 0000-0002-0021-1815

Notes

The authors declare no competing financial interest.

■ ACKNOWLEDGMENTS

We would like to thank Dr. Boning Wu for his help in conducting DFT calculation. We also want to thank Samantha Hung for her measurement of absorption spectrum of MeSCN in 1-methylimidazole. This work was supported by the Division of Chemical Sciences, Geosciences, and Biosciences, Office of Basic Energy Sciences of the U.S. Department of Energy through Grant No. DEFG03-84ER13251 (R.Y., MDF), and in part by the Air Force Office of Scientific Research under AFOSR Award No. FA9550-16-1-0104 (C.Y., MDF, and the ultrafast IR spectrometer).

■ REFERENCES

(1) Barthel, J. M. G.; Krienke, H.; Kunz, W. Physical Chemistry of Electrolyte Solutions: Modern Aspects. In *Topics in Physical Chemistry*, edited by Deutsche Bunsengesellschaft; Steinkopff, Darmstadt/Springer: New York, 1998; Vol. *5*.

(2) Marcus, Y. Effect of Ions on the Structure of Water: Structure Making and Breaking. *Chem. Rev.* **2009**, *109*, 1346−1370.

(3) Mamontov, E.; De Francesco, A.; Formisano, F.; Laloni, A.; Sani, L.; Leu, B. M.; Said, A. H.; Kolesnikov, A. I. Water Dynamics in a Lithium Chloride Aqueous Solution Probed by Brillouin Neutron and X-ray Scattering. *J. Phys.: Condens. Matter* **2012**, *24*, No. 064102.

(4) Terpstra, P.; Combes, D.; Zwick, A. Effect of Salts on Dynamics of Water - a Raman-Spectroscopy Study. *J. Chem. Phys.* **1990**, *92*, 65−70.

DOI: 10.1021/acs.jpcb.8b08743
J. Phys. Chem. B 2018, 122, 10582−10592

(5) Giammanco, C. H.; Wong, D. B.; Fayer, M. D. Water Dynamics in Divalent and Monovalent Concentrated Salt Solutions. *J. Phys. Chem. B* **2012**, *116*, 13781−13792.
(6) Smith, J. D.; Saykally, R. J.; Geissler, P. L. The Effect of Dissolved Halide Anions on Hydrogen Bonding in Liquid Water. *J. Am. Chem. Soc.* **2007**, *129*, 13847−13856.
(7) Tielrooij, K. J.; Garcia-Araez, N.; Bonn, M.; Bakker, H. J. Cooperativity in Ion Hydration. *Science* **2010**, *328*, 1006−1009.
(8) Marcus, Y.; Hefter, G. Ion pairing. *Chem. Rev.* **2006**, *106*, 4585−4621.
(9) Sun, Z.; Zhang, W. K.; Ji, M. B.; Hartsock, R.; Gaffney, K. J. Contact Ion Pair Formation between Hard Acids and Soft Bases in Aqueous Solutions Observed with 2DIR Spectroscopy. *J. Phys. Chem. B* **2013**, *117*, 15306−15312.
(10) Kiefer, L. M.; Kubarych, K. J. NOESY-Like 2D-IR Spectroscopy Reveals Non-Gaussian Dynamics. *J. Phys. Chem. Lett.* **2016**, *7*, 3819−3824.
(11) Lee, K. K.; Park, K. H.; Kwon, D.; Choi, J. H.; Son, H.; Park, S.; Cho, M. Ion-pairing Dynamics of Li^+ and SCN^- in Dimethylformamide Solution: Chemical Exchange Two-dimensional Infrared Spectroscopy. *J. Chem. Phys.* **2011**, *134*, No. 064506.
(12) Park, K. H.; Choi, S. R.; Choi, J. H.; Park, S.; Cho, M. Real-Time Probing of Ion Pairing Dynamics with 2DIR Spectroscopy. *ChemPhysChem* **2010**, *11*, 3632−3637.
(13) Dougherty, D. A. Cation-pi Interactions in Chemistry and Biology: A New View of Benzene, Phe, Tyr, and Trp. *Science* **1996**, *271*, 163−168.
(14) Song, L. X.; Pan, S. Z.; Zhu, L. H.; Wang, M.; Du, F. Y.; Chen, J. Molecule-Ion Interaction and Its Effect on Coordination Interaction. *Inorg. Chem.* **2011**, *50*, 2215−2223.
(15) Kashyap, H. K.; Biswas, R. Solvation Dynamics of Dipolar Probes in Dipolar Room Temperature Ionic Liquids: Separation of Ion-Dipole and Dipole-Dipole Interaction Contributions. *J. Phys. Chem. B* **2010**, *114*, 254−268.
(16) Borisenko, V.; Burns, D. C.; Zhang, Z. H.; Woolley, G. A. Optical Switching of Ion-dipole Interactions in a Gramicidin Channel Analogue. *J. Am. Chem. Soc.* **2000**, *122*, 6364−6370.
(17) Kwon, Y.; Park, S. Complexation Dynamics of CH_3SCN and Li^+ in Acetonitrile Studied by Two-Dimensional Infrared Spectroscopy. *Phys. Chem. Chem. Phys.* **2015**, *17*, 24193−24200.
(18) Moilanen, D. E.; Wong, D.; Rosenfeld, D. E.; Fenn, E. E.; Fayer, M. D. Ion-Water Hydrogen-bond Switching Observed with 2D IR Vibrational Echo Chemical Exchange Spectroscopy. *Proc. Natl. Acad. Sci. U.S.A.* **2009**, *106*, 375−380.
(19) Ji, M.; Odelius, M.; Gaffney, K. J. Large Angular Jump Mechanism Observed for Hydrogen Bond Exchange in Aqueous Perchlorate Solution. *Science* **2010**, *328*, 1003−1005.
(20) Suo, L.; Borodin, O.; Gao, T.; Olguin, M.; Ho, J.; Fan, X. L.; Luo, C.; Wang, C. S.; Xu, K. "Water-in-salt" Electrolyte Enables High-voltage Aqueous Lithium-ion Chemistries. *Science* **2015**, *350*, 938−943.
(21) Cheng, X. B.; Zhang, R.; Zhao, C. Z.; Zhang, Q. Toward Safe Lithium Metal Anode in Rechargeable Batteries: A Review. *Chem. Rev.* **2017**, *117*, 10403−10473.
(22) Harsányi, I.; Pusztai, L. Hydration Structure in Concentrated Aqueous Lithium Chloride Solutions: A Reverse Monte Carlo based Combination of Molecular Dynamics Simulations and Diffraction Data. *J. Chem. Phys.* **2012**, *137*, No. 204503.
(23) Tromp, R. H.; Neilson, G. W.; Soper, A. K. Water-Structure in Concentrated Lithium-Chloride Solutions. *J. Chem. Phys.* **1992**, *96*, 8460−8469.
(24) Petit, L.; Vuilleumier, R.; Maldivi, P.; Adamo, C. Ab Initio Molecular Dynamics Study of a Highly Concentrated LiCl Aqueous Solution. *J. Chem. Theory Comput.* **2008**, *4*, 1040−1048.
(25) Fecko, C. J.; Eaves, J. D.; Loparo, J. J.; Tokmakoff, A.; Geissler, P. L. Ultrafast Hydrogen-Bond Dynamics in the Infrared Spectroscopy of Water. *Science* **2003**, *301*, 1698−1702.
(26) Asbury, J. B.; Steinel, T.; Kwak, K.; Corcelli, S. A.; Lawrence, C. P.; Skinner, J. L.; Fayer, M. D. Dynamics of Water Probed with Vibrational Echo Correlation Spectroscopy. *J. Chem. Phys.* **2004**, *121*, 12431.
(27) Asbury, J. B.; Steinel, T.; Stromberg, C.; Corcelli, S. A.; Lawrence, C. P.; Skinner, J. L.; Fayer, M. D. Water Dynamics: Vibrational Echo Correlation Spectroscopy and Comparison to Molecular Dynamics Simulations. *J. Phys. Chem. A* **2004**, *108*, 1107−1119.
(28) Yan, C.; Thomaz, J. E.; Wang, Y. L.; Nishida, J.; Yuan, R. F.; Breen, J. P.; Fayer, M. D. Ultrafast to Ultraslow Dynamics of a Langmuir Monolayer at the Air/Water Interface Observed with Reflection Enhanced 2D IR Spectroscopy. *J. Am. Chem. Soc.* **2017**, *139*, 16518−16527.
(29) Shim, S. H.; Zanni, M. T. How to Turn Your Pump-probe Instrument into a Multidimensional Spectrometer: 2D IR and Vis Spectroscopies via Pulse Shaping. *Phys. Chem. Chem. Phys.* **2009**, *11*, 748−761.
(30) Kumar, S. K. K.; Tamimi, A.; Fayer, M. D. Comparisons of 2D IR Measured Spectral Diffusion in Rotating Frames using Pulse Shaping and in the Stationary Frame using the Standard Method. *J. Chem. Phys.* **2012**, *137*, No. 184201.
(31) Kwak, K.; Park, S.; Finkelstein, I. J.; Fayer, M. D. Frequency-Frequency Correlation Functions and Apodization in Two-Dimensional Infrared Vibrational Echo Spectroscopy: A New Approach. *J. Chem. Phys.* **2007**, *127*, No. 124503.
(32) Kwak, K.; Rosenfeld, D. E.; Fayer, M. D. Taking Apart the Two-Dimensional Infrared Vibrational Echo Spectra: More Information and Elimination of Distortions. *J. Chem. Phys.* **2008**, *128*, No. 204505.
(33) Park, S.; Fayer, M. D. Hydrogen Bond Dynamics in Aqueous NaBr Solutions. *Proc. Natl. Acad. Sci. U.S.A.* **2007**, *104*, 16731−16738.
(34) Zheng, J.; Kwak, K.; Asbury, J. B.; Chen, X.; Piletic, I. R.; Fayer, M. D. Ultrafast Dynamics of Solute-Solvent Complexation Observed at Thermal Equilibrium in Real Time. *Science* **2005**, *309*, 1338−1343.
(35) Zheng, J.; Kwak, K. W.; Xie, J.; Fayer, M. D. Ultrafast Carbon-Carbon Single-bond Rotational Isomerization in Room-Temperature Solution. *Science* **2006**, *313*, 1951−1955.
(36) Ishikawa, H.; Kwak, K.; Chung, J. K.; Kim, S.; Fayer, M. D. Direct Observation of Fast Protein Conformational Switching. *Proc. Natl. Acad. Sci. U.S.A.* **2008**, *105*, 8619−8624.
(37) Kwak, K.; Zheng, J.; Cang, H.; Fayer, M. D. Ultrafast 2D IR Vibrational Echo Chemical Exchange Experiments and Theory. *J. Phys. Chem. B* **2006**, *110*, 19998−20013.
(38) Tokmakoff, A. Orientational Correlation Functions and Polarization Selectivity for Nonlinear Spectroscopy of Isotropic Media. 1. Third Order. *J. Chem. Phys.* **1996**, *105*, 1−12.
(39) Tao, T. Time-Dependent Fluorescence Depolarization and Brownian Rotational Diffusion Coefficients of Macromolecules. *Biopolymers* **1969**, *8*, 609−632.
(40) Yuan, R.; Yan, C.; Tamimi, A.; Fayer, M. D. Molecular Anion Hydrogen Bonding Dynamics in Aqueous Solution. *J. Phys. Chem. B* **2015**, *119*, 13407−13415.
(41) Yamada, S. A.; Thompson, W. H.; Fayer, M. D. Water-Anion Hydrogen Bonding Dynamics: Ultrafast IR Experiments and Simulations. *J. Chem. Phys.* **2017**, *146*, No. 234501.
(42) Wang, C. C.; Pecora, R. Time-Correlation Functions for Restricted Rotational Diffusion. *J. Chem. Phys.* **1980**, *72*, 5333−5340.
(43) Lipari, G.; Szabo, A. Effect of Librational Motion on Fluorescence Depolarization and Nuclear Magnetic-Resonance Relaxation in Macromolecules and Membranes. *Biophys. J.* **1980**, *30*, 489−506.
(44) Sannigrahi, A. B.; Kar, T.; Niyogi, B. G.; Hobza, P.; Schleyer, P. V. The Lithium Bond Reexamined. *Chem. Rev.* **1990**, *90*, 1061−1076.
(45) Smith, A. M.; Lee, A. A.; Perkin, S. The Electrostatic Screening Length in Concentrated Electrolytes Increases with Concentration. *J. Phys. Chem. Lett.* **2016**, *7*, 2157−2163.
(46) Frisch, M. J.; Trucks, G. W.; Schlegel, H. B.; Scuseria, G. E.; Robb, M. A.; Cheeseman, J. R.; Scalmani, G.; Barone, V.; Petersson, G. A.; Nakatsuji, H.;et al. *Gaussian 16*, revision B.01; Gaussian, Inc.: Wallingford, CT, 2016.
(47) Wu, B.; Yamashita, Y.; Endo, T.; Takahashi, K.; Castner, E. W. Structure and Dynamics of Ionic Liquids: Trimethylsilylpropyl-

DOI: 10.1021/acs.jpcb.8b08743
J. Phys. Chem. B 2018, 122, 10582−10592

Substituted Cations and Bis(sulfonyl)amide Anions. *J. Chem. Phys.* **2016**, *145*, No. 244506.
(48) Hu, C.-M.; Zwanzig, R. Rotational Friction Coefficients for Spheroids with the Slipping Boundary Condition. *J. Chem. Phys.* **1974**, *60*, 4354−4357.

DOI: 10.1021/acs.jpcb.8b08743
J. Phys. Chem. B 2018, 122, 10582−10592